Two-nucleon correlation effects in knockout reactions from ^{12}C

E. C. Simpson and J. A. Tostevin
Department of Physics, Faculty of Engineering and Physical Sciences, University of Surrey, Guildford, Surrey GU2 7XH, United Kingdom
(Received 7 December 2010; published 26 January 2011)

Reactions that involve the direct and sudden removal of a pair of like or unlike nucleons from a fast projectile beam by a light target nucleus are considered. Specifically, we study the three two-nucleon removal channels from ^{12}C that populate final states in the ^{10}Be, ^{10}B, and ^{10}C reaction residues. The calculated two-nucleon removal cross sections and the residue momentum distributions are compared with available high-energy data at 250, 1050, and 2010 MeV per nucleon, i.e., data that are inclusive with respect to the bound final states of the residues. The measured np removal cross sections only are significantly greater than the values calculated, suggesting that the reaction mechanism observes enhanced np spatial correlations compared to those present in the shell-model wave functions.

DOI: 10.1103/PhysRevC.83.014605 PACS number(s): 24.50.+g, 25.70.Mn, 21.10.Pc

I. INTRODUCTION

There is an extensive literature on the development and the use of high-energy electron-induced knockout of both one or two nucleons from the ground states of stable nuclei as probes of nucleonic correlations and of pair correlations. Relevant and recent reviews include references [1–4] that cite the essential experimental developments and data sets; see, also, the citations in [5]. Quite recently, new conclusions have been drawn regarding the observation of enhanced short-ranged correlations (SRC) between nucleon-nucleon pairs from $(e, e'pN)$ experiments on a carbon target [5]. Specifically, measurements that selected high momentum transfer and large missing momentum events from the few-body final-state phase space found evidence that np pairs were more than an order of magnitude more prevalent than like-nucleon pairs in this selection; this was deduced from the corresponding $(e, e'np)$ and $(e, e'2p)$ yields. The probabilities of these high-relative-momentum two-nucleon components have been computed, using the microscopic ground-state wave functions from *ab initio* variational Monte Carlo calculations, for systems with masses $A \leqslant 8$ [6,7] and, using a linked cluster expansion, for $A \geqslant 12$ [8]. These computations involve the wave functions of the nucleons over the entire volume of the nuclei concerned. These theoretical studies strongly suggest that the tensor force (in the spin $S = 1$, isospin $T = 0$, np channel) plays the major role in generating these enhanced np spatial correlations and their associated high-relative-momenta signatures in the two-nucleon density distribution. In such $(e, e'pN)$ measurements, the specific final-state phase-space selection (of high-relative-momentum, back-to-back two-nucleon events) provides the leverage and the amplification of the short-ranged pair-correlation sensitivity.

The behavior of the wave functions of single nucleons and of pairs of nucleons (in a mass $A + 2$ projectile) can also be probed if the nucleons are removed (suddenly) in fast collisions with a light target nucleus. Within this strong-interaction probe case, the sensitivity is now to the nuclear wave functions at, and near, the nuclear surface. Such processes are also referred to as one- and two-nucleon knockout (or removal) reactions. These direct reaction mechanisms, combined with γ-decay spectroscopy to determine the final state of the reaction residues and their momentum distributions, are being actively exploited as a spectroscopic tool to study the evolution of nucleonic single-particle structure near the two (often very displaced) Fermi surfaces of exotic nuclei. They are proving to be robust techniques (see, e.g., [9–11]).

Unlike the final-state-exclusive measurements in electron-induced reactions, observables in such nuclear-induced fast nucleon removal reactions are inclusive with respect to the final states of the removed nucleon(s) and the fate of the struck light target nucleus. The cross sections are thus relatively large. Measurements usually consist of the total removal reaction yield, often the momenta of the fast, forward-traveling projectile-like residues, and sometimes the differential yields to the ground and bound excited states of the mass $A + 1$ or mass A residual nuclei; the latter are obtained by γ-ray spectroscopy. However, in such collisions between the projectile and a light composite target nucleus, such as beryllium or carbon, the reaction is *geometrically* very selective [17], and the removal of two nucleons will be enhanced if nucleon pairs have a strong spatial correlation (and localization) in the projectile ground state. An interesting question, therefore, is whether like and unlike two-nucleon removal under such conditions also exhibits any evidence of enhanced np over nn and pp spatial correlations on a longer length scale than implied by the (SRC) observations of the electron knockout data. Here, the spatial (geometrical) selectivity of the reaction mechanism would provide the leverage and probe of the presence of spatially localized pairs and evidence of an enhanced np correlation.

Experimental data are available in the form of high-energy, primary beam measurements of the inclusive cross sections to the bound states of the residues after np, nn, and pp removal [12,13]. We will show that these data reveal a significant enhancement of unlike-pair yields σ_{-np} relative to those σ_{-nn} and σ_{-pp} for like-nucleon pairs, the enhancement being significantly greater than would be expected (trivially) from the numbers of such pair combinations available.

The removal of two (well-bound) nucleons of the deficient species from asymmetric nuclei has been shown to proceed

as a direct reaction [14]. A description of the reaction making use of configuration-mixed shell-model wave functions and elastic and inelastic breakup contributions to the removal cross section has been shown to reproduce experiment [15]. Such calculations have also recently been extended to describe the reaction residue momentum distributions [16,17], where it was shown that the shapes and widths of the residue momentum distributions are indicative of both the total angular-momentum (I) and the total orbital-angular-momentum components ($\boldsymbol{L} = \boldsymbol{\ell}_1 + \boldsymbol{\ell}_2$) of the removed nucleon pair [18].

Here, we will exploit the eikonal reaction model in the isospin formalism [15,17,19] for the removal of like ($T = 1$) and unlike ($T = 0, 1$) nucleon pairs. We also discuss the possible role of indirect population of the residue final states of interest, i.e., by single-nucleon knockout paths that populate particle unbound states of the intermediate mass $A + 1$ system. Such indirect paths severely limit the number of systems that, in the absence of an empirical means to distinguish between direct and indirect knockout events, may be studied quantitatively with unlike-pair knockout. These indirect contributions to final-state yields are expected, in general, to be large in np removal from asymmetric systems [20] where one or the other of the nucleon thresholds will be at relatively low excitation energy.

Attractive np removal test cases thus suggest symmetric light nuclei, e.g., ^{12}C or ^{16}O. For such less-massive cases, one must, however, consider core recoil effects in the reaction and the analogous center-of-mass corrections to the (fixed-center) shell-model two-nucleon amplitudes. Both are expected to affect, in detail, the absolute magnitudes of the cross sections. These are discussed here. Regardless of these two (relatively small) effects, comparisons of the relative like- and unlike-pair knockout yields may be made.

In Sec. II, we outline the specific features of the reactions using ^{12}C projectiles. The necessary formalism has been presented elsewhere and will only be outlined in Sec. III, exploiting the notation used in previous work. The calculated results for ^{12}C are discussed in Sec. IV and a summary is given in Sec. V.

II. CARBON-INDUCED REACTIONS

Our current expectation is that a quantitative discussion of pair-correlation effects can only be made when the residue final states are populated predominantly via a single-step direct reaction. It is thus vital to select examples that minimize the indirect (evaporative) contributions to the reaction yield, and that we assume can not (at present) be distinguished from the direct reactions of interest. We must therefore consider systems with large (and symmetric) nucleon separation thresholds, such that the single-nucleon removal strength to particle unbound states will be weak. For the same reason, we require the projectile nucleus to be relatively light to minimize population of the (bound) final residue states via the removal of deeply bound (nonvalence) nucleons. Ideally, any experiment would also measure single-nucleon and like-pair removal, in addition to the unlike-pair removal, in order to verify shell- and reaction-model predictions for the distribution of single-nucleon spectroscopic strength and for the direct $T = 1$ pair knockout. These considerations severely constrain the potential candidates, the best examples being ^{12}C and ^{16}O. The former of these will be considered in detail here. The choice of an $N = Z$ projectile poses the additional (experimental) complication of distinguishing the mass A residue from the incident beam, with the residue and projectile having identical mass-to-charge ratios.

Consideration of two-nucleon knockout from ^{12}C is valuable for two reasons. First, its shell-model description and that of the residual nuclei ^{10}C, ^{10}Be, and ^{10}B are extensively studied and, so, establish a valuable point of reference. Second, the existing experimental cross sections for two-nucleon knockout from ^{12}C [12,13] are accurate to $\approx$10% and were taken at high energies, where the eikonal model used here is at its most reliable. The experimental data were obtained using reactions of a carbon beam on a carbon target at 250, 1050, and 2100 MeV per nucleon incident energies. These show an expected enhancement of the ^{10}B production cross sections (np removal) over those for the nn (to ^{10}C) and pp (to ^{10}Be) removal reactions (see Table III). The significance of this observed enhancement is quantified here.

In addition to two-nucleon removal, single-nucleon removal cross sections were also measured at high energy (and previously studied theoretically, see Ref. [10]). These verify the expectation, from the shell model, that the majority of single-particle removal strength is exhausted in transitions to final states lying below the nucleon separation thresholds of ^{11}C and ^{11}B. This point will be developed further in later sections. The relevant one- and two-nucleon (and α-particle) separation thresholds are illustrated in Fig. 1.

The simplest of the three two-nucleon removal cases is two-neutron (nn) removal, leading to the ^{10}C residual nucleus. This has only two bound final states below the first proton threshold, the 0^+ ground state and a 2^+ excited state at 3.354 MeV [21]. The level scheme of ^{10}Be, the residual nucleus

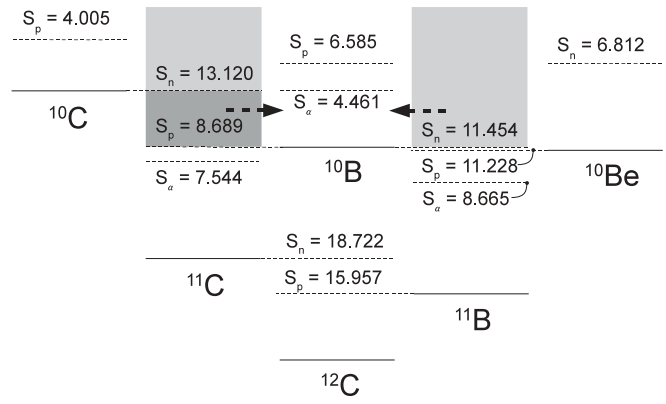

FIG. 1. One- and two-nucleon and α-particle separation thresholds relevant to nucleon removal reactions from ^{12}C. The ^{12}C two-nucleon separation energies are $S_{2p} = 27.184$, $S_{2n} = 31.184$, and $S_{np} = 27.412$ MeV. Proton evaporation from the single-neutron removal residue ^{11}C would be expected to be the largest indirect pathway, but the shell-model calculations suggest very little spectroscopic strength to states above 8.689 MeV in ^{11}C.

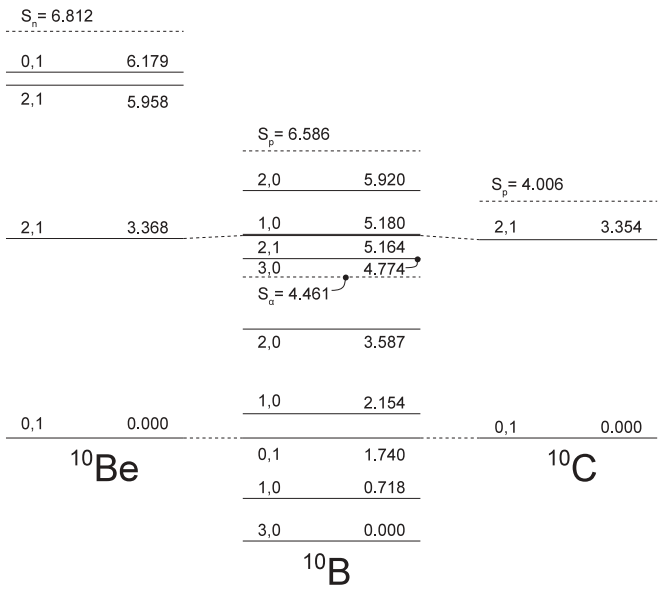

FIG. 2. States of the mass $A = 10$ residues populated in the two-nucleon knockout. The spin and isospin labels (J_f, T_f) are indicated. All states included are of positive parity. Levels assumed to be part of the isospin multiplet are connected by dashed lines. The lowest particle thresholds are also indicated. States above the α-particle threshold in ^{10}B are expected to decay via α emission, with the exception of the 5.164 MeV, $T = 1$, $J^\pi = 2^+$ state, which has an 84% γ-decay branch.

in the pp removal case, is only slightly more complex. We must consider population of the 0^+ ground state, the 2^+ states at 3.368 and 5.958 MeV, and a second 0^+ state at 6.179 MeV, all below the neutron threshold of 6.812 MeV. The most complicated final state is that for ^{10}B, the np knockout residue. The p-shell-model calculations used include even-parity states up to a maximum of spin 3. For ^{10}B, we have shown states up to the proton separation threshold, however, the low α-particle separation threshold means that the $T = 0$ states at 4.774 (3^+), 5.180 (1^+), and 5.920 MeV (2^+) are reported to decay (with branching ratios of near 100%) by α emission. We will show the cross sections for population of these states, but will assume that they do not contribute to the calculated ^{10}B yield. The $T = 1$, 2^+(5.184 MeV) state is reported to have a 16% α-emission branch. These ^{10}B states are illustrated in Fig. 2. We note that the ^{10}B spectrum also contains several negative-parity states, which are not expected to be populated by the nucleon-removal reaction mechanism.

Direct, unlike-pair removal cross sections are expected to be larger than those for like pairs. Assuming the simplest p-shell $\pi[0p_{3/2}]^4\nu[0p_{3/2}]^4$ structure for ^{12}C, the pn format two-nucleon amplitudes (TNAs) for pair removal to a residue final state with spin J_f are given by the appropriate coefficients of fractional parentage, with the value $\sqrt{2J_f + 1}$. The cross sections to a given final state, being proportional to the square of these TNA, suggest unlike:like two-nucleon inclusive-cross-section ratios $\sigma_{-np}/\sigma_{-2N} = 16/6 \approx 2.7$, if all strength leads to bound final states. The same result is obtained from the counting of available valence-nucleon pairs.

The primary motivation for this paper is that this simple combinatorics expectation is not corroborated by the available data; the ratio σ_{np}/σ_{pp} (σ_{np}/σ_{nn}) from the experiments at 250, 1050, and 2100 MeV/nucleon are 8.1 (8.9), 5.3 (6.3), and 6.0 (8.5), respectively [13], with the observed enhancement of the np removal cross section being significantly larger than expected.

Clearly, our simple estimate, from the number of available pairs of each type, assumes that all of the removal strength leads to bound configurations in the residue of interest, which is not the case, and part of the enhancement noted above may be attributable to this (channel-dependent) fraction of events leading to particle unbound states. Here, we seek to address this question quantitatively by the use of a direct reaction model for two-nucleon removal. Specifically, our aims are to quantify (i) whether this enhancement is accounted for by those two-nucleon correlations that are included in the truncated, p-space shell-model calculation, and (ii) to make a simple estimate of the contributions one might reasonably expect from indirect reaction pathways in this model picture.

III. FORMALISM

A. Two-nucleon overlap

The formalism used is based on that developed in Refs. [15,17]. Isospin-format TNAs will be used and are expected to offer a good description of the light symmetric systems considered here. Thus, in the unlike-pair removal case, we assume a common set of nucleon orbital wave functions, to be discussed in the following.

We evaluate the cross sections for transitions from the projectile initial (ground) state i, with spin (J_i, M_i), to particular residue final states f. The residue is assumed to be a spectator in the sudden reaction description and its state is not coupled to the reaction dynamics. The direct reaction will then probe the two-nucleon overlap. We denote the A-body final states by $\Phi^{(F)}(A)$, where the label $F \equiv (f, M_f)$ includes the angular-momentum projection M_f. The two-nucleon wave function (two-nucleon overlap) of the removed nucleons 1 and 2 is written as $\Psi_i^{(F)}(1, 2)$, where

$$\begin{aligned}\Psi_i^{(F)} &\equiv \Psi^{(F)}_{J_i M_i T_i \tau_i}(1,2) \\ &\equiv \langle \Phi^{(F)}(A) | \Psi_i(A,1,2) \rangle \\ &= \sum_{I\mu T\alpha} C_\alpha^{IT} (I\mu J_f M_f | J_i M_i) \\ &\quad \times (T\tau T_f \tau_f | T_i \tau_i) \left[\overline{\psi_{\beta_1}(1) \otimes \psi_{\beta_2}(2)} \right]^{T\tau}_{I\mu} . \end{aligned} \quad (1)$$

Here, the set of available active two-nucleon configurations, with counter α, consists of particular pairs of single-particle orbitals $[\beta_1, \beta_2]$, where the index $\beta = (n\ell j)$ denotes the state's spherical quantum numbers. The C_α^{IT} are the two-nucleon amplitudes that express the parentage of the residue final state, when coupled to a particular two-nucleon configuration α, in the projectile ground state. Here, as elsewhere, these are taken from a truncated-basis shell-model calculation.

Expressed in LS coupling, the antisymmetrized two-nucleon wave function of Eq. (1) is

$$\left[\overline{\psi_{\beta_1}(1)\otimes\psi_{\beta_2}(2)}\right]^{T\tau}_{I\mu} = D_\alpha \hat{j}_1\hat{j}_2 \sum_{L\Lambda S\Sigma\lambda_1\lambda_2} (\ell_1\lambda_1\ell_2\lambda_2|L\Lambda)(L\Lambda S\Sigma|I\mu)\,\hat{L}\hat{S}\,\chi_{S\Sigma}(1,2)\chi_{T\tau}(1,2)$$
$$\times\left[\phi^{\lambda_1}_{\ell_1 j_1}(1)\phi^{\lambda_2}_{\ell_2 j_2}(2) - (-)^{S+T}\phi^{\lambda_1}_{\ell_1 j_1}(2)\phi^{\lambda_2}_{\ell_2 j_2}(1)\right]\begin{Bmatrix}\ell_1 & s & j_1\\ \ell_2 & s & j_2\\ L & S & I\end{Bmatrix}, \quad (2)$$

with $D_\alpha = 1/\sqrt{2(1+\delta_{\beta_1\beta_2})}$. The angular-momentum and isospin couplings used are summarized in Fig. 3. The nucleon wave functions $\phi^\lambda_{\ell j}(i)$ are

$$\phi^\lambda_{\ell j}(i) = u_\beta(r_i)Y_{\ell\lambda}(\hat{\boldsymbol{r}}_i). \quad (3)$$

We note that no explicit account is taken of additional (short-, medium-, or long-range) correlations other than those contained within the shell-model description, and that enter Eq. (1). These are seen to arise from (a) antisymmetry and angular-momentum coupling of the nucleon pair, and (b) the (shell-model) two-nucleon overlap, via the weights and phases of the contributing TNAs. If there are significant additional strong-interaction generated pair correlations, which are missing from our description, then we might expect empirical cross sections to deviate significantly (and be enhanced) relative to the shell-model correlated model used here.

B. Center-of-mass corrections to the TNA

Spectroscopic factors calculated within the fixed-center shell-model basis require a center-of-mass correction factor to be applied [22]. Essentially, the shell-model two-nucleon overlaps are calculated relative to the center of mass of all $A+2$ nucleons and not relative to the remaining A nucleons. Such corrections were discussed by Pinkston [23–25] (see, also, Ref. [26]). In previous, predominantly sd-shell applications, such corrections were expected to be small but, for the examples discussed here, they may be more significant, particularly when one has an ambition to compare absolute cross sections with experiment.

In the simplest (harmonic-oscillator) limit, the requirement is to multiply the shell-model TNAs by a factor $[(A+2)/A]^{N/2}$, with N the number of oscillator quanta of the orbitals of the active nucleons. In the present case of ^{12}C$(-2N)$, this would enhance all cross sections by ≈20%, independent of the reaction channel and the residue. Thus, conclusions regarding the *relative strengths* of the different two-nucleon removal channels will be unaffected and we do not apply these corrections. Clearly, a more complete understanding will be necessary for a precise consideration of the absolute cross sections.

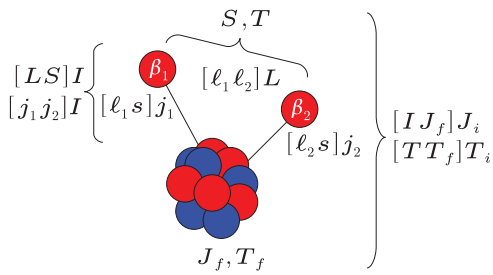

FIG. 3. (Color online) Diagram of the angular-momentum and isospin couplings, and the coupling orders assumed. Specifically, the LS couplings used in this paper are presented.

C. Reaction dynamics and approximations

We exploit eikonal reaction dynamics with the required nucleon- and residue-target S matrices calculated in the optical limit of Glauber theory [27,28]. These elastic S matrices are thus calculated assuming that the residue and nucleons travel on straight-line paths through the interaction field of the target. The residue-target S matrices are calculated by double folding their densities with an effective nucleon-nucleon (NN) interaction. The absorptive nature of these interactions naturally localizes the reaction to the projectile surface [17]. A detailed derivation of the two-nucleon removal cross section is presented elsewhere [15], as is the formalism for their momentum distributions [17,18]. These are not reproduced here.

The key approximations are as follows. The removal of nucleons is sudden, i.e., their coordinates are assumed to vary slowly compared to the timescale of the reaction, and can be assumed frozen during the interaction. In previous work, we have also (reasonably) made the no-recoil (heavy residue) approximation in the diffraction-stripping terms of the removal cross section [15]; i.e., we have assumed coincidence of the residue and projectile centers of mass and impact parameters $b_c \approx b$. These core recoil effects will certainly introduce corrections for the lighter residues in this work; however, as will be quantified later, at the high projectile energies considered here, these diffractive-stripping terms contribute a significantly smaller fraction of the cross section than the two-nucleon stripping terms. Thus, recoil will have a relatively minor effect on the calculated removal cross sections and the discussion of this paper. This effect will be fully quantified in future work.

IV. NUCLEON KNOCKOUT FROM ^{12}C

A. Methodology

The experimental information available consists of final-state inclusive cross sections to bound states of the mass

$A = 11, 10$ residues and some associated residue momentum distribution information. We are able to identify each known positive-parity final state ($A = 10$) and negative-parity final state ($A = 11$) with a well-defined shell-model state. The shell-model calculations were performed with OXBASH [29]. We will consider the results when using the WBP interaction [30], and also compare these with the PJT interaction [31] outcomes, in the p-shell-model space. The former interaction was used in previous work on nucleon removal from ^{12}C [10]. The shell-model spectroscopic factors C^2S and the two-nucleon spectroscopic amplitudes C_α^{IT}, as in Eq. (1), were calculated for each residue final state. To discuss possible indirect processes, we must consider the population of highly excited, unbound states in the single-nucleon removal cases.

The p-shell-model space allows removal of nucleons from the active $p_{3/2}$ and $p_{1/2}$ single-particle orbitals. The radial wave functions used to describe these nucleonic states are calculated in a Woods-Saxon potential well. The radius and diffuseness parameters were fixed to be $r_0 = 1.310$ fm and $a = 0.55$ fm, as were used in the single-nucleon knockout analysis of Ref. [10]. In addition, we include a spin-orbit potential of depth $V_{so} = 6$ MeV. The ground-state to ground-state nn, pp, and np separation energies S_{2N} from ^{12}C are 31.841, 27.184, and 27.41 MeV, respectively. The nucleon bound-state wave functions for each reaction and transition, with final-state excitation energy E_f, were calculated using effective nucleon separation energies of

$$B_f = S_N + E_f \tag{4}$$

for single-nucleon removal and

$$B_f = (S_{2N} + E_f)/2 \tag{5}$$

for each nucleon in two-nucleon removal. In the np removal case, we assumed a common set of radial wave functions for the neutrons and protons. These were calculated as above but assumed that each nucleon carried a charge of $0.5e$.

The required nucleon- and residue-target S matrices were calculated using the optical limit of Glauber theory [27], i.e., by double folding each constituent particle and target density with an effective nucleon-nucleon interaction. The essential input parameters, given the dominance of the stripping mechanism, are the free nn ($\equiv pp$) and np cross sections, taken from the parametrization of Ref. [32] and the residue and target densities. The former are given in Table I. The effective NN interaction was assumed to be zero range, represented by a δ function, and the real:imaginary forward-scattering amplitude ratios α_{nn} and α_{np} were obtained from a polynomial fit to the values tabulated in Ref. [33]. These are listed in Table I for the three energies of interest. The point-nucleon density distributions of the target and the residues were assumed to have Gaussian shapes, with root-mean-squared (rms) radii consistent with Glauber-model analyses of the measured interaction cross sections [34]. For simplicity, we assume a single-matter rms radius for each mass nucleus; for ^{12}C target and $A = 11$ and $A = 10$ residues, the mass radii were 2.32, 2.11, and 2.30 fm, respectively. The latter value is that quoted for ^{10}Be in Ref. [34].

TABLE I. Nucleon-nucleon effective interaction parameters used for the calculation of the nucleon- and residue-target S matrices.

Energy (MeV/u)	σ_{nn} (mb)	σ_{np} (mb)	α_{nn}	α_{np}
250	22.3	36.6	0.94	0.49
1050	49.6	41.6	−0.08	−0.46
2100	63.9	46.5	−0.20	−0.47

B. Single-nucleon removal cross sections

We first briefly review the single-nucleon removal results, as were previously discussed in Ref. [10]. Of particular interest here is the proportion of spectroscopic strength exhausted below particle separation thresholds, and hence the shell-model prediction of single-particle strength lying above the nucleon separation thresholds. For the WBP interaction, 3.93 units of spectroscopic strength are associated with states below these thresholds, with the remaining 0.07 fragmented over many states above 10 MeV in excitation. Calculations using the PJT interaction distribute the single-particle spectroscopic strength similarly, with 3.97 units associated with states below the mass $A = 11$ nucleon thresholds.

The results for single-nucleon removal are very similar to those presented previously [10]. The small differences can be traced to our inclusion of a spin-orbit term in the nucleon-bound-states potential. The detailed decomposition of the single-particle cross sections for each final state into their stripping and diffraction components, for the beam energy of 2100 MeV/nucleon, are shown in Table II. A discussion of the single-nucleon shell-model suppression factors can be found in Ref. [10]. Here, we simply note that the theoretical cross section overestimates the experiment by approximately a factor of 2, consistent with the results from electron-induced proton knockout [4].

TABLE II. Single-nucleon knockout cross sections (mb) for the ^{12}C projectile incident on a carbon target at 2100 MeV per nucleon. The single-nucleon removal cross sections presented, σ_{-1N}, include both the spectroscopic C^2S (from the WBP interaction) and center-of-mass correction factors (here 12/11). The results are very similar to those of Ref. [10]. The inclusion here of the nucleon-bound-states spin-orbit potential accounts for the very minor differences observed.

Residue	J_f^π	σ_{str}	σ_{dif}	C^2S	σ_{-1N}
^{11}C	$3/2^-$	20.50	2.17	3.16	78.18
	$1/2^-$	18.45	1.81	0.58	12.82
	$3/2^-$	18.74	1.81	0.19	4.26
				Sum	95.36
				Expt.	46.50 ± 2.30
^{11}B	$3/2^-$	21.11	2.30	3.16	80.70
	$1/2^-$	18.86	1.90	0.58	13.14
	$3/2^-$	19.09	1.88	0.19	4.35
				Sum	98.81
				Expt.	53.80 ± 2.70

With regards to possible indirect contributions to np knockout, we can estimate an upper bound, assuming that the remaining shell-model C^2S strength (of 0.07) from both proton and neutron channels will populate the np residue indirectly. Doing so, we obtain an indirect contribution of $\approx$3 mb. It is, however, unlikely that this entire residual p-shell strength would lead to the ^{10}B residue. The removal of deeply bound $0s_{1/2}$ nucleons may also lead to the ^{10}B residue, although the single-particle cross section will be significantly smaller than those presented in Table II due to the stronger binding. We return to this indirect contribution discussion in the following section.

C. Two-nucleon removal cross sections

The stripping mechanism component of the two-like-nucleon removal cross sections from ^{12}C has previously discussed in Ref. [35]. Here, we extend these results to consider the stripping-diffraction mechanism contributions and consideration of unlike-pair knockout to confront the available experimental data quantitatively. As was discussed earlier, disregarding the configuration mixing inherent in the shell-model two-nucleon overlap, we might expect the unlike-pair knockout yields to be enhanced by approximately a factor of 16/6 over those for like-nucleon knockout from the counting of available $[p_{3/2}]^2$ pairs. As was also pointed out, this zeroth-order estimate assumes all of the two-nucleon strength will fall below the first particle-emission thresholds. In practice, the number of bound states and the fraction of the removal strength leading to bound states is different for the three residues. The lowest relevant particle separation thresholds are as follows: ^{10}C, $S_p = 4.006$ MeV; ^{10}Be $S_n = 6.586$ MeV; ^{10}B, $S_\alpha = 4.461$ MeV. Both the number of pair combinations and the distribution of two-particle removal strength should be reasonably accounted for when using the shell-model two-nucleon amplitudes.

Results for the inclusive cross sections for two-nucleon removal from ^{12}C to the three residues, at beam energies of 250, 1050, and 2100 MeV per nucleon, are given in Table III. The final-state-exclusive like and unlike two-nucleon removal cross sections, and their decomposition with the contributing reaction mechanisms (i.e., stripping $\sigma_{\rm str}$, diffraction-stripping $\sigma_{\rm ds}$, and estimated diffraction $\sigma_{\rm dif}$) are shown in Table IV for the 2100 MeV per nucleon case and when using the WBP interaction TNAs. Table III shows the calculated theoretical like-pair removal cross sections $\sigma_{\rm th}$, to ^{10}C and ^{10}Be, are in reasonable agreement with the experimental data $\sigma_{\rm exp}$ of Refs. [12,13].

TABLE IV. Like- and unlike-two-nucleon removal cross sections (in mb) for a ^{12}C projectile incident on a carbon target at 2100 MeV per nucleon. The excitation energies E_f of each final state are shown in Fig. 2. The TNAs used were calculated using the WBP interaction. The sums show the accumulated cross sections that lead to the ground state and the γ-decaying bound excited states of the mass $A = 10$ residues.

Residue	J^π_f	T	$\sigma_{\rm str}$	$\sigma_{\rm ds}$	$\sigma_{\rm dif}$	σ_{-2N}
^{10}C	0^+	1	1.59	0.64	0.06	2.30
	2^+	1	1.96	0.71	0.06	2.74
					Sum	5.04
					Expt.	4.11 ± 0.22
^{10}Be	0^+	1	1.65	0.68	0.07	2.40
	2^+	1	2.02	0.74	0.07	2.83
	2^+	1	0.88	0.32	0.03	1.23
	0^+	1	0.04	0.01	0.00	0.06
					Sum	6.52
					Expt.	5.81 ± 0.29
^{10}B	3^+	0	5.11	2.00	0.20	7.30
	1^+	0	2.47	1.01	0.10	3.58
	0^+	1	1.62	0.66	0.07	2.35
	1^+	0	1.81	0.69	0.07	2.57
	2^+	0	0.63	0.24	0.02	0.89
	3^{+a}	0	1.14	0.43	0.04	1.62
	2^{+b}	1	1.99	0.72	0.07	2.33
	1^{+a}	0	0.30	0.10	0.01	0.41
	2^{+a}	0	0.75	0.28	0.03	1.05
					Sum	19.02
					Expt.	35.10 ± 3.40

[a]States decay by α emission with a 100% branching ratio.
[b]State decays by α emission with a 16% α branch.

From Table IV, we note that, at this projectile energy, the two-nucleon stripping (absorption) term $\sigma_{\rm str}$, accounts for $\approx$70% of the calculated cross section. The cross sections for those $T = 1$ states common to all three residues, namely, the first 0^+ and 2^+ states, are also essentially equal, with the minor differences in the calculations arising from the small differences in the separation energies for each system.

For np removal to ^{10}B, the cross sections are shown for the nine p-shell shell-model final states below the first nucleon threshold. However, the first $2^+, T = 1$ state is known to decay by α emission with a branch of $I_\alpha = 16\%$. For this state, this branching has been accounted for in the σ_{-2N} value presented. The cross sections are also shown for the three highest energy

TABLE III. Theoretical and experimental cross sections for two-nucleon knockout from ^{12}C, for projectile energies of 250, 1050, and 2100 MeV per nucleon. All cross sections are in mb. The TNAs used were calculated using the WBP interaction.

Energy	^{10}Be			^{10}C			^{10}B		
MeV/u	$\sigma_{\rm th}$	$\sigma_{\rm exp}$	$\sigma_{\rm exp}/\sigma_{\rm th}$	$\sigma_{\rm th}$	$\sigma_{\rm exp}$	$\sigma_{\rm exp}/\sigma_{\rm th}$	$\sigma_{\rm th}$	$\sigma_{\rm exp}$	$\sigma_{\rm exp}/\sigma_{\rm th}$
250 [12]	7.48	5.88 ± 9.70	0.79 ± 1.30	5.80	5.33 ± 0.81	0.92 ± 0.14	21.57	47.50 ± 2.42	2.20 ± 0.11
1050 [13]	6.62	5.30 ± 0.30	0.80 ± 0.05	5.13	4.44 ± 0.24	0.87 ± 0.05	19.27	27.90 ± 2.20	1.45 ± 0.11
2100 [13]	6.52	5.81 ± 0.29	0.89 ± 0.04	5.04	4.11 ± 0.22	0.82 ± 0.04	19.02	35.10 ± 3.40	1.84 ± 0.18

$T = 0$ states, but these states are reported to decay (with $I_\alpha = 100\%$) by α emission. These cross sections are not included in the summed ^{10}B yield. These exclusive ^{10}B cross sections will be discussed further in Sec. IV D and in Fig. 5, in connection with their associated momentum distributions. We note here that if one uses the PJT shell-model interaction TNAs, then the summed ^{10}B yield is 18.73 mb, compared to the 19.02 mb shown in Table IV. The calculated inclusive cross sections are thus robustly determined within the p-shell-model space calculations.

As for the present like-nucleon cases, previous analyses of like-two-nucleon removal data for asymmetric sd-shell nuclei have indicated a suppression of the measured values compared to the theoretical model being used. Previously, this factor was of order $R_s(2N) = \sigma_{\rm exp}/\sigma_{\rm th} \approx 0.5$. The present higher energy, like-nucleon calculations suggest a larger value of R_s (see Table III). As was noted earlier, these calculations do not include center-of-mass (recoil) corrections to the two-nucleon amplitudes or the reaction dynamics. The latter will introduce minor corrections to the diffraction-stripping term only, which contributes to the cross sections at the 30% level. Since the magnitude of these effects is not quantified here, we do not draw detailed conclusions regarding the absolute cross sections and $R_s(2N)$ for ^{12}C, although the required corrections will not be large. We show the ratio $\sigma_{\rm exp}/\sigma_{\rm th}$ in Table III to compare the results for the relative strengths of the different two-nucleon removal channels. All three channels will be affected similarly by these corrections.

We note that, in the full calculations, there is an enhancement in the theoretical np removal cross sections for all three incident energies, already in excess of the $16/6 \approx 2.7$ ratio from the counting of pairs. The calculated np:pp cross-section ratios $\sigma_{np}/\sigma_{pp} \approx 2.9$ are marginally smaller than those for the np:nn case ≈ 3.8, largely reflecting the different fractions of spectroscopic strength to bound states in the two like-nucleon cases (there being only two bound states in ^{10}C).

Since the magnitudes of the pp and nn removal cross sections are reasonably described, our expectation is that the cross sections to the states of the $T = 1$ isospin multiplet in ^{10}B are similarly well determined. However, an independent measurement of these cross sections would provide a useful verification of the direct nature of the reaction. Thus, within the direct reaction model used, we must attribute the cross-section deficit to the calculated yields of the $T = 0$ final states. We also note that, while the energy dependence of the like-pair removal cross sections is reasonably reproduced by the theoretical calculations, there is some discrepancy in the unlike-pair removal channel, with the result that the degree of underestimation varies with energy. The theoretical values for both the like- and unlike-pair removal decrease moderately with increasing projectile energy. This said, there remain considerable variations from the experimental np knockout cross sections.

D. Momentum distributions

In addition to the fragment production cross-section measurements of Ref. [13], residue momentum distributions were also measured [36]. Except for the case of two-proton removal using a ^{9}Be target, the experimental data sets have been published only as the widths of Gaussian fits to the experimental data. Here, we denote these as Δ_G. Further, the published width parameters were the averages of data measured for several targets (Be, CH_2, C, Al, Cu, Ag, and Pb), although it was observed that, within the accuracy of the experiment, there was no dependence on the target mass above a 5% level. These references do not discuss the thicknesses of the targets used, or of the momentum resolution of the incident beam, both of which could broaden the measured widths. We assume that, since the data are for high-energy (stable) beams, this experimental broadening of the width is negligible.

Following, and to enable comparisons with the results of Ref. [36], we fit our calculated (projectile rest frame) *inclusive* residue momentum distributions with Gaussian functions. The two-nucleon-stripping and diffractive-stripping mechanisms are expected to yield very similar residue momentum distributions [17], and here we present calculations for pure stripping events, scaled to match the mechanism-inclusive cross section for each final state. In general, these calculated final-state-inclusive residue momentum distributions are very close to Gaussian shapes. This is not the case, however, for the individual (exclusive) residue final states, particularly those of higher spin, which have a broader and flatter distribution near the central value $\kappa_c = 0$ MeV/c. The results are collected and compared in Table V and are, encouragingly, in good agreement.

The calculated residue momentum distributions for two-proton removal are compared to the data in Fig. 4, with the data having been scanned from Fig. 1 of Ref. [36]. The data provided are for a beryllium target, while the calculations assume a carbon target. Any differences in the momentum distributions are expected to be very small for these two light targets. Both the exclusive contributions from the four ^{10}Be final states involved and their sum are shown. The figure shows clearly that the inclusive Gaussian-like distribution is formed of exclusive cross sections of very different widths for the different final states. Thus, residue momentum distributions for these individual final states would be of considerable

TABLE V. Projectile rest frame residue momentum distribution widths Δ_G (for reactions at 2100 MeV per nucleon) obtained by fitting Gaussian profiles to the experimental [36] and theoretical (this work) inclusive distributions to bound final states. The TNAs used were calculated using the WBP interaction. The data of Ref. [36] are the average widths from data for several targets (see text). The calculated values are for a carbon target only.

Residue	$\Delta_G^{\rm expt}$	$\Delta_G^{\rm th}$
^{11}B	106 ± 4	99
^{11}C	103 ± 4	100
^{10}Be	129 ± 4	127
^{10}B	134 ± 3	132
^{10}C	121 ± 6	120

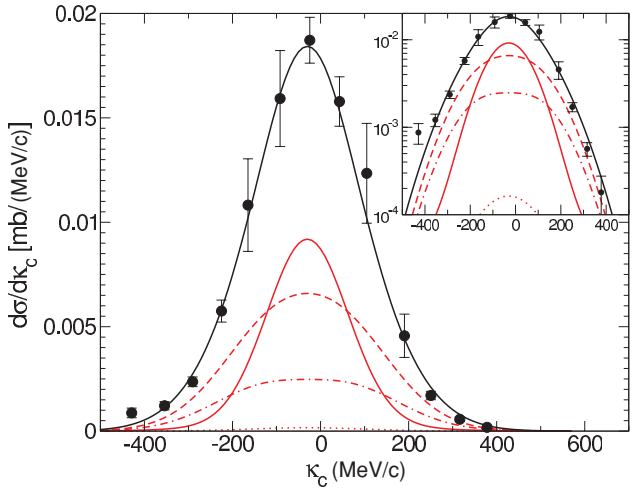

FIG. 4. (Color online) Comparison of measured and calculated ^{10}Be projectile frame residue momentum distributions. The red curves show the ^{10}Be final-state-exclusive results for the ground state (solid line), 2^+_1 (dashed line), 2^+_2 (dot-dashed line), and 0^+_2 (dotted line). The inclusive cross section, and their sum, is shown by the black solid line that passes through the data points. The data are for a ^{9}Be target, whereas the calculations assume a ^{12}C target. The calculations have been offset by -30 MeV/c and have been scaled to match the experimental two-proton removal cross section on the ^{9}Be target of 5.97 mb. The TNAs used were calculated using the WBP interaction.

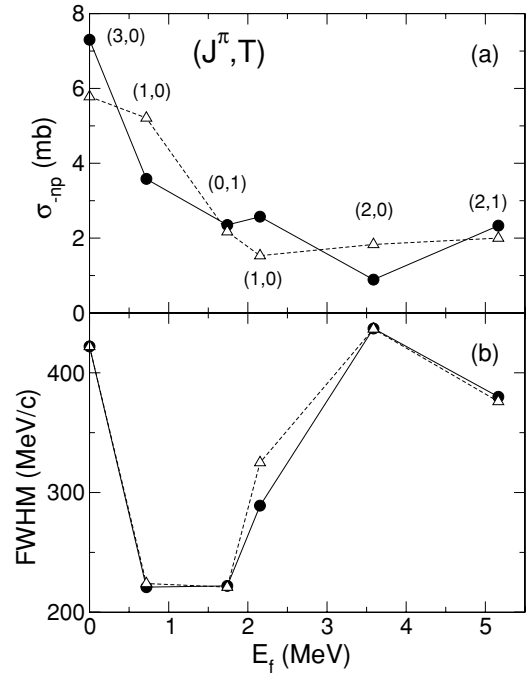

FIG. 5. Calculated exclusive cross sections (a) and full-width at half-maximum widths of the momentum distributions (b) for the six γ-decaying final states of the ^{10}B residues, for reactions at 2100 MeV per nucleon. The TNAs used were obtained using the WBP interaction (solid lines and solid points) and the PJT interaction (dashed lines and open points). The significant variations predicted (i) for the widths of the momentum distributions to the different final states, and (ii) in the sensitivity of the ^{10}B, $T = 0$ final state yields to the effective interaction used are evident.

value in validating, or revealing deficiencies in, the details of the shell-model wave functions and TNAs used here, including our description of the reaction as a direct single-step process.

Details of these calculated full-width at half-maximum (FWHM) widths in the case of *np* removal at 2100 MeV per nucleon for the six γ-decaying final states of ^{10}B, are shown in Fig. 5. Results from both the WBP (solid lines and filled points) and PJT (dashed lines and open points) shell-model interaction TNA are shown. The widths from the two interactions are remarkably similar for all transitions, indicative that the LS contributions to each final state are very similar [18]. The momentum distributions for the first and second $T = 0$, 1^+ states of ^{10}B were also presented in Fig. 3 of Ref. [18], calculated from the WBP interaction. The corresponding exclusive cross sections (upper panel of the figure) also show very similar trends for the two shell-model interactions. They differ in detail, however, particularly with regard to the ratio of the cross sections to the ground (3^+, $T = 0$) and first excited (1^+, $T = 0$) states. We note also that the two interactions predict very similar cross sections in the two $T = 1$ states, with the differences being more evident in the $T = 0$ states yields. Once again, this suggests interesting information would be gained from exclusive-final-states yields.

The predicted final-state-dependent variations of the FWHM widths from the model used also offer considerable scope for further testing of the reaction inputs, the shell-model wave functions used, and the nucleon-nucleon correlations content of these wave functions.

V. SUMMARY

We have considered, in detail, theoretical expectations for the cross sections of two-nucleon removal reactions from ^{12}C incident on a carbon target, at beam energies of 250, 1050, and 2100 MeV per nucleon. The calculated inclusive cross sections for two-like-nucleon ($T = 1$) removal are broadly consistent with available experimental data. For *np* pair removal, the analogous $T = 1$, ^{10}B final states are also shown to be insensitive to the shell-model interactions used. The calculated inclusive *np* pair removal cross sections at all energies *underestimate* the data by approximately a factor of 2. Theoretical calculations of the widths of the final-state-inclusive residue momentum distributions, on the other hand, are consistent with the available experimental data, including for the *np* removal channel.

Further measurements of final-state-exclusive cross sections and residue momentum distributions would allow a much more detailed scrutiny and validation of the direct nature of the reaction, including the identification of any indirect reaction components. The calculated *np* removal cross sections to the $T = 0$, ^{10}B final states were also shown to have sensitivity to the shell-model effective interaction used, for example, the ratio of the calculated cross sections to the ^{10}B ground (3^+, $T = 0$) and first (1^+, $T = 0$) excited states.

The overall conclusion from this analysis is that the existing data suggest that the $T = 0$, np spatial correlations present in the wave functions used are insufficient. We have shown that exclusive measurements would offer a means to interrogate these shell-model inputs, in particular the np channel, $T = 0$ wave functions, and the direct reaction mechanism predictions in considerable detail.

A similar two-nucleon knockout study can also be performed using an ^{16}O projectile, for which np pair knockout using electromagnetic probes has been measured [37,38] and supports the SRC observations for ^{12}C. In this case, the ^{14}O residue is also of interest, given that only the 0^+ ground state is bound, and where the results of Refs. [13,36] indicate a correspondingly small cross section and a narrow momentum distribution, consistent with theoretical expectations. Additionally, possible $2\hbar\omega$ components in the ^{16}O ground-state wave function add interest to the magnitudes of the absolute cross sections in this case.

ACKNOWLEDGMENTS

The assistance of B. A. Brown and P. Fallon is acknowledged. This work was supported by the United Kingdom Science and Technology Facilities Council (STFC) under Grant No. ST/F012012. E.C.S. is grateful for support from the United Kingdom Engineering and Physical Sciences Research Council (EPSRC) under Grant No. EP/P503892/1.

[1] A. E. L. Dieperink and P. K. A. de Witt Huberts, Annu. Rev. Nucl. Part. Sci. **40**, 239 (1990).
[2] V. R. Pandharipande, I. Sick, and P. K. A. de Witt Huberts, Rev. Mod. Phys. **68**, 981 (1997).
[3] Omar Benhar, Donal Day, and Ingo Sick, Rev. Mod. Phys. **80**, 189 (2008).
[4] W. H. Dickhoff and C. Barbieri, Prog. Part. Nucl. Phys. **52**, 377 (2004).
[5] R. Subedi *et al.*, Science **320**, 1476 (2008).
[6] R. Schiavilla, R. B. Wiringa, Steven C. Pieper, and J. Carlson, Phys. Rev. Lett. **98**, 132501 (2007).
[7] R. B. Wiringa, R. Schiavilla, Steven C. Pieper, and J. Carlson, Phys. Rev. C **78**, 021001 (2008).
[8] M. Alvioli, C. Ciofi degli Atti, and H. Morita, Phys. Rev. Lett. **100**, 162503 (2008).
[9] P. G. Hansen and J. A. Tostevin, Annu. Rev. Nucl. Part. Sci. **53**, 219 (2003).
[10] B. A. Brown, P. G. Hansen, B. M. Sherrill, and J. A. Tostevin, Phys. Rev. C **65**, 061601 (2002).
[11] J. R. Terry, D. Bazin, B. A. Brown, J. Enders, T. Glasmacher, P. G. Hansen, B. M. Sherrill, and J. A. Tostevin, Phys. Rev. C **69**, 054306 (2004).
[12] J. M. Kidd, P. J. Lindstrom, H. J. Crawford, and G. Woods, Phys. Rev. C **37**, 2613 (1988).
[13] P. J. Lindstrom, D. E. Greiner, H. H. Heckman, Bruce Cork, and F. S. Bieser, LBL Report No. LBL3650, 1975 (unpublished); also tabulated in D. L. Olson, B. L. Berman, D. E. Greiner, H. H. Heckman, P. J. Lindstrom, and H. J. Crawford, Phys. Rev. C **28**, 1602 (1983).
[14] D. Bazin *et al.*, Phys. Rev. Lett. **91**, 012501 (2003).
[15] J. A. Tostevin and B. A. Brown, Phys. Rev. C **74**, 064604 (2006).
[16] E. C. Simpson, J. A. Tostevin, D. Bazin, B. A. Brown, and A. Gade, Phys. Rev. Lett. **102**, 132502 (2009).
[17] E. C. Simpson, J. A. Tostevin, D. Bazin, and A. Gade, Phys. Rev. C **79**, 064621 (2009).
[18] E. C. Simpson and J. A. Tostevin, Phys. Rev. C **82**, 044616 (2010).
[19] J. A. Tostevin, G. Podolyák, B. A. Brown, and P. G. Hansen, Phys. Rev. C **70**, 064602 (2004).
[20] E. C. Simpson and J. A. Tostevin, Phys. Rev. C **79**, 024616 (2009).
[21] D. R. Tilley *et al.*, Nucl. Phys. A **745**, 155 (2004).
[22] A. E. L. Dieperink *et al.*, Phys. Rev. C **10**, 543 (1974).
[23] W. T. Pinkston, Nucl. Phys. A **269**, 281 (1976).
[24] W. T. Pinkston, Nucl. Phys. A **291**, 342 (1977).
[25] W. T. Pinkston *et al.*, Nucl. Phys. A **330**, 91 (1979).
[26] J. M. Bang *et al.*, Phys. Rep. **125**, 253 (1985).
[27] R. J. Glauber, in *Lectures in Theoretical Physics*, edited by W. E. Brittin and L. G. Dunham (Interscience, New York, 1959), Vol. 1, p. 315.
[28] J. S. Al Khalili, J. A. Tostevin, and I. J. Thompson, Phys. Rev. C **54**, 1843 (1996).
[29] B. A. Brown *et al.*, MSU-NSCL Report No. 1289, 2004 (unpublished).
[30] E. K. Warburton and B. A. Brown, Phys. Rev. C **46**, 923 (1992).
[31] R. E. Julies, W. A. Richter, and B. A. Brown, South African J. Phys. **15**, 35 (1992).
[32] S. K. Charagi and S. K. Gupta, Phys. Rev. C **41**, 1610 (1990).
[33] L. Ray, Phys. Rev. C **20**, 1857 (1979).
[34] A. Ozawa *et al.*, Nucl. Phys. A **693**, 32 (2001).
[35] J. A. Tostevin, P. Batham, G. Podolyák, and I. J. Thompson, Nucl. Phys. A **746**, 166c (2004).
[36] D. E. Greiner *et al.*, Phys. Rev. Lett. **35**, 152 (1975).
[37] D. G. Middleton *et al.*, Eur. Phys. J. A **29**, 261 (2006).
[38] D. G. Middleton *et al.*, Eur. Phys. J. A **43**, 137 (2010).